

# Non-negative $K_{DP}$ Estimation by Monotone Increasing $\Phi_{DP}$ Assumption below Melting Layer

Takeshi Maesaka<sup>1</sup>, Koyuru Iwanami<sup>1</sup> and Masayuki Maki<sup>1</sup>

<sup>1</sup>National Research Institute for Earth Science and Disaster Prevention  
3-1 Tennodai, Tsukuba, Ibaraki, 305-0006, Japan  
Corresponding E-mail: maesaka@bosai.go.jp

(Dated: 3 June 2012)



Takeshi Maesaka

## 1. Introduction

Dual-polarimetric weather radar becomes prevalent for Quantitative Precipitation Estimation (QPE) in recent years. Especially, Ministry of Land, Infrastructure, Transport and Tourism (MLIT), Japan started deploying X-band Dual-polarimetric radar network around great urban areas and local major cities for a real-time monitoring of heavy precipitation. Now 27 radars in 11 areas have already been deployed, and more 8 radars will be installed by FY 2013. This real-time QPE system generates a precipitation intensity data with the horizontal resolution of 250 m, and the data are updated every 1 minute (Maesaka et al. 2011). In this system, the precipitation intensity ( $R$ ) is calculated not from radar reflectivity ( $Z_h$ ) but from specific differential phase ( $K_{DP}$ ) for heavy or moderate rainfalls. Moreover,  $K_{DP}$  is used for attenuation corrections of  $Z_h$  and differential reflectivity ( $Z_{DR}$ ). So the recent QPE progress in X-band radar is due to that the  $K_{DP}$  becomes available.

The  $K_{DP}$  is not directly observed by radar system (not a result of I/Q signal processing), but is calculated by a derivative of a differential phase ( $\Phi_{DP}$ ) with respect to range. Because the observed  $\Phi_{DP}$  contaminated by noise, and the differentiation works as a high-pass filter, it is difficult to retrieve the original  $K_{DP}$  caused by meteorological phenomena. Thus local linear or polynomial regressions are generally used to estimate the original  $K_{DP}$ ; however, these procedures make a spatial resolution of the  $K_{DP}$  coarse. Furthermore, a differential backscatter phase ( $\delta$ ) overlaps in the observed  $\Phi_{DP}$ . It is not negligible if large precipitation particles exist in the radar beam. Sarchilli et al. (1993) estimated the differential backscatter phase from the attenuation-corrected  $Z_{DR}$ . Hubbert and Bringi (1995) proposed an iterative filtering technique to remove the backscatter phase from the observed  $\Phi_{DP}$ . There are also recent studies on the robust  $K_{DP}$  estimation with high spacial resolution, e.g., Wang and Chandrasekar (2009) and Otto and Russchenberg (2011).

At present, the stable version algorithms of  $K_{DP}$  estimation in MLIT and National Research Institute for Earth Science and Disaster Prevention (NIED) are based on the classical methods: the iterative filtering and the local linear regression (Maesaka et al. 2011). These algorithms sometimes estimate a negative  $K_{DP}$  in rainfall (below melting layer), though the positive  $K_{DP}$  is expected for pure rain drops. The negative  $K_{DP}$  tends to be estimated in a weak rainfall area and far-side of heavy precipitation. The former negative  $K_{DP}$  is caused by the noise of  $\Phi_{DP}$ , and the latter is influenced by the differential backscatter phase. This fake  $K_{DP}$  is a problem in the MLIT and NIED algorithms, because it disable the rainfall estimation and the attenuation correction.

In this paper, a new  $K_{DP}$  estimation method is proposed by assuming the monotone increasing  $\Phi_{DP}$  below melting layer. The  $K_{DP}$  estimated by this new method always takes a positive value.

## 2. Method

In this method, we assume a monotone increasing  $\Phi_{DP}$  with respect to the range from radar ( $r$ ). So the use of this method is limited in rainfall (below melting layer). The monotone increasing  $\Phi_{DP}$  is fitted to the observed  $\Phi_{DP}$  by a variational approach.

### 2.1 Quality Control

At first, the observed data in or higher than melting layer should be rejected, because this method is only available for pure rainfall. Of course, a precipitation particle identification can be used by using the dual-polarimetric information; however it is not completely robust at present. The zero degree level information from sounding data or numerical simulations, and the assumed melting layer depth (e.g., 500 m or 1000 m) may be useful for this purpose.

Then no precipitation (low S/N ratio) data, ground and point clutter data, and outlier data are rejected. Finally  $\Phi_{DP}$  unfolding should be performed in case the  $\Phi_{DP}$  exceeds a expression range of  $360^\circ$  or  $180^\circ$ .

### 2.2 Boundary Conditions

Figure 1 show a schematic range profile of the observed and analyzed  $\Phi_{DP}$  in this method. This method needs boundary conditions  $\Phi_{near}$  and  $\Phi_{far}$  at the nearest and farthest ranges, respectively, as shown in Fig. 1. The final solution of  $\Phi_{DP}$  varies between these boundary conditions.

The nearest boundary  $\Phi_{\text{near}}$  is determined by the linear regression (Line LR-N in Fig. 1), which is calculated with the specified number (e.g., 30) of available data (excluding the rejected data by the quality control) from the nearest range. If the slope of the regression line is positive, the value of the regression line at the nearest range ( $r_{\text{near}}$ ) is used for the boundary condition. Otherwise, the averaged value of the available data is used. The farthest boundary  $\Phi_{\text{far}}$  is determined in the same manner. The specified number of available data from the farthest range are used for the linear regression (Line LR-F in Fig. 1). The value of the regression line at the farthest range ( $r_{\text{far}}$ ) is used for the positive slope case, or the averaged value is used. In the case of Fig. 1, the value of the regression line at the nearest range (the averaged value at the farthest range) is used because the slope of the regression line is positive (negative), respectively.

### 2.3 Cost Function

Now the observed and final solution of differential phase are denoted as  $\Psi_i$  and  $(\Phi_{\text{DP}})_i$ , respectively, where the suffix  $i$  is an index of range ( $i = 0, 1, 2, \dots, N$ ). Here we define  $\phi_i$  as,

$$\phi_i = (\Phi_{\text{DP}})_i - \Phi_{\text{near}}. \quad (1)$$

The definition of  $K_{\text{DP}}$  is,

$$K_{\text{DP}} = \frac{1}{2} \frac{\partial \Phi_{\text{DP}}}{\partial r}, \quad (2)$$

so (1) can be written as,

$$\phi_0 = 0, \quad (3)$$

$$\phi_i = 2 \sum_{j=0}^{i-1} (K_{\text{DP}})_j \Delta r \quad (i = 1, 2, 3, \dots, N), \quad (4)$$

where  $\Delta r$  is a range gate width. We introduce  $k_i$  as,

$$k_i^2 = 2(K_{\text{DP}})_i \Delta r, \quad (5)$$

because we assume that the  $K_{\text{DP}}$  always takes a positive value. With (5), (4) can be written as,

$$\phi_i = \sum_{j=0}^{i-1} k_j^2 \quad (i = 1, 2, 3, \dots, N). \quad (6)$$

On the other hand, the reverse version of  $\phi_i$  (as  $\phi'_i$  shown in Fig. 1) is also defined as,

$$\phi'_i = \Phi_{\text{far}} - (\Phi_{\text{DP}})_i. \quad (7)$$

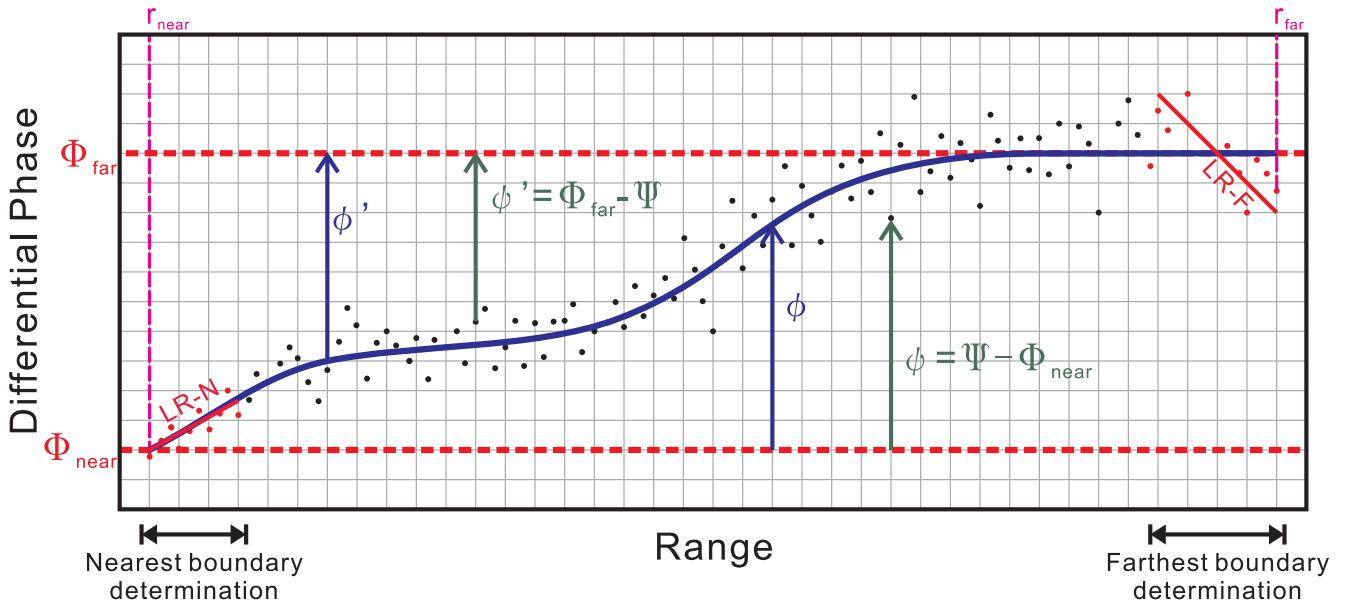


Fig. 1 Schematic range profile of the observed and analyzed  $\Phi_{\text{DP}}$  in this method. Horizontal and vertical axes indicate the range from radar and the differential phase, respectively. Dots indicate the observed differential phase ( $\Psi$ ) at the range, and blue solid line is a final solution of the differential phase in this method. Broken red lines are boundary conditions of the differential phases ( $\Phi_{\text{near}}$  and  $\Phi_{\text{far}}$ ) at the nearest and farthest ranges ( $r_{\text{near}}$  and  $r_{\text{far}}$ ), respectively. Lines LR-N and LR-F are linear regression lines to determine the boundary conditions  $\Phi_{\text{near}}$  and  $\Phi_{\text{far}}$ , respectively.

Then the following equations are deduced in the same manner.

$$\begin{aligned}\phi'_i &= 2 \sum_{j=i+1}^N (K_{DP})_j \Delta r \\ &= \sum_{j=i+1}^N k_j^2 \quad (i = 0, 1, 2, \dots, N-1),\end{aligned}\quad (8)$$

$$\phi'_N = 0. \quad (9)$$

The differences between the observed differential phase and the boundary conditions are also defined as,

$$\psi_i = \Psi_i - \Phi_{\text{near}}, \quad (10)$$

$$\psi'_i = \Phi_{\text{far}} - \Psi_i. \quad (11)$$

Here a cost function  $J$  to be minimized is defined as,

$$J = J_{\text{obs}} + J'_{\text{obs}} + J_{\text{lpf}}, \quad (12)$$

$$J_{\text{obs}} = \frac{1}{N} \sum_{i=1}^N (\phi_i - \psi_i)^2, \quad (13)$$

$$J'_{\text{obs}} = \frac{1}{N} \sum_{i=0}^{N-1} (\phi'_i - \psi'_i)^2, \quad (14)$$

$$J_{\text{lpf}} = \frac{1}{N+1} C_{\text{lpf}} \sum_{i=0}^N \left( \frac{\partial^2 k_i}{\partial r^2} \right)^2. \quad (15)$$

$J_{\text{obs}}$  and  $J'_{\text{obs}}$  are mean square errors between the observed and analyzed differential phases. These terms of the cost function make the analyzed differential phase fitted to the observed one.  $J_{\text{lpf}}$  is a mean square of a Laplacian of  $k$ , and works as a low pass filter.  $C_{\text{lpf}}$  in (15) is a control parameter of the low pass filter.

We regard the range profile of  $k$  which minimizes the cost function as the final solution in this problem. The final  $K_{DP}$  is calculated from  $k$  by (5). To minimize the cost function, we used the Broyden-Fletcher-Goldfarb-Shanno (BFGS) method, which is a kind of numerical optimizations. The BFGS method needs the derivative of the cost function with respect to the independent variables, and it is written as,

$$\frac{\partial}{\partial k_i} J = \frac{\partial}{\partial k_i} (J_{\text{obs}} + J'_{\text{obs}}) + \frac{\partial}{\partial k_i} J_{\text{lpf}}, \quad (16)$$

$$\frac{\partial}{\partial k_i} (J_{\text{obs}} + J'_{\text{obs}}) = \begin{cases} \frac{4k_0}{N} \sum_{i=1}^N (\phi_i - \psi_i) & (i = 0), \\ \frac{4k_i}{N} \sum_{i=0}^{i-1} (\phi'_i - \psi'_i) + \frac{4k_i}{N} \sum_{i=i+1}^N (\phi_i - \psi_i) & (i = 1, 2, 3, \dots, N-1), \\ \frac{4k_N}{N} \sum_{i=0}^{N-1} (\phi'_i - \psi'_i) & (i = N), \end{cases} \quad (17)$$

$$\frac{\partial}{\partial k_i} J_{\text{lpf}} = \frac{2}{N+1} C_{\text{lpf}} \frac{\partial^2}{\partial r^2} \left( \frac{\partial^2 k_i}{\partial r^2} \right). \quad (18)$$

Figure 2 shows the example profiles of the observed and the analyzed differential phases. The observed profile (blue line in Fig. 2) is contaminated by the noise, and includes the significant backscatter phase around the range of 17 km, where big hails might exist at that time. The analyzed profile (red line in Fig. 2) well corresponds with the observed one with the constraint of the monotone increasing.

Figure 3 shows the  $K_{DP}$  profiles calculated from the observed differential phase shown in Fig. 2. The  $K_{DP}$  calculated by the classical method (the local linear regression with the window width of 1 km; blue line in Fig. 3) fluctuates around  $0 \text{ } ^\circ \text{ km}^{-1}$  (e.g., in the ranges of 5 km – 10 km and 20 km – 30 km), and sometimes takes negative values. Especially, a large negative value is estimated just behind the significant backscatter phase (around the range of 17 km in Fig. 2). On the other hand, the  $K_{DP}$  calculated by this method ( $C_{\text{lpf}} = 1 \times 10^{11}$ ) does not show such a fluctuation and negative values.

#### 2.4 Dependency of $C_{\text{lpf}}$

The parameter  $C_{\text{lpf}}$  in (15) controls how the low pass filter effects. Here the dependency of the  $C_{\text{lpf}}$  to the low pass filter is examined by assuming that  $k$  is a periodic function with the wavelength of  $L$  as,

$$k = a \sin \left( \frac{2\pi}{L} r \right). \quad (19)$$

Substituting (19) for (5), we get,

$$K_{DP} = \frac{a^2}{4\Delta r} \left\{ 1 - \cos \left( \frac{2\pi}{L/2} r \right) \right\}. \quad (20)$$

So the wavelength of the  $K_{DP}$  is  $L/2$  under the condition of (19). Substituting (19) for (15), we also get,

$$\begin{aligned} J_{lpf} &\sim \lim_{r \rightarrow \infty} \frac{1}{r} \left[ \int_0^r \left( \frac{\partial^2 k}{\partial r^2} \right)^2 dr \right] \\ &= \frac{16\pi^4 a^2}{L^4} \lim_{r \rightarrow \infty} \left[ \frac{1}{r} \int_0^r \sin^2 \left( \frac{2\pi}{L} r \right) dr \right] \\ &= \frac{8\pi^4 a^2}{L^4}. \end{aligned} \quad (21)$$

On the other hand,  $J_{obs}$  and  $J'_{obs}$  are the mean square errors of the differential phase observation. Defining these terms as  $\sigma_{obs}^2$ , we get,

$$J_{obs} + J'_{obs} = 2\sigma_{obs}^2. \quad (22)$$

If the term  $J_{lpf}$  is larger (smaller) than the term  $(J_{obs} + J'_{obs})$ , the result becomes smoother (more detailed). So from (21) and (22), a roughly estimated cut-off wavelength of the low pass filter is written as,

$$L \sim \pi \sqrt{\frac{2a}{\sigma_{obs}}} C_{lpf}^{\frac{1}{4}}. \quad (23)$$

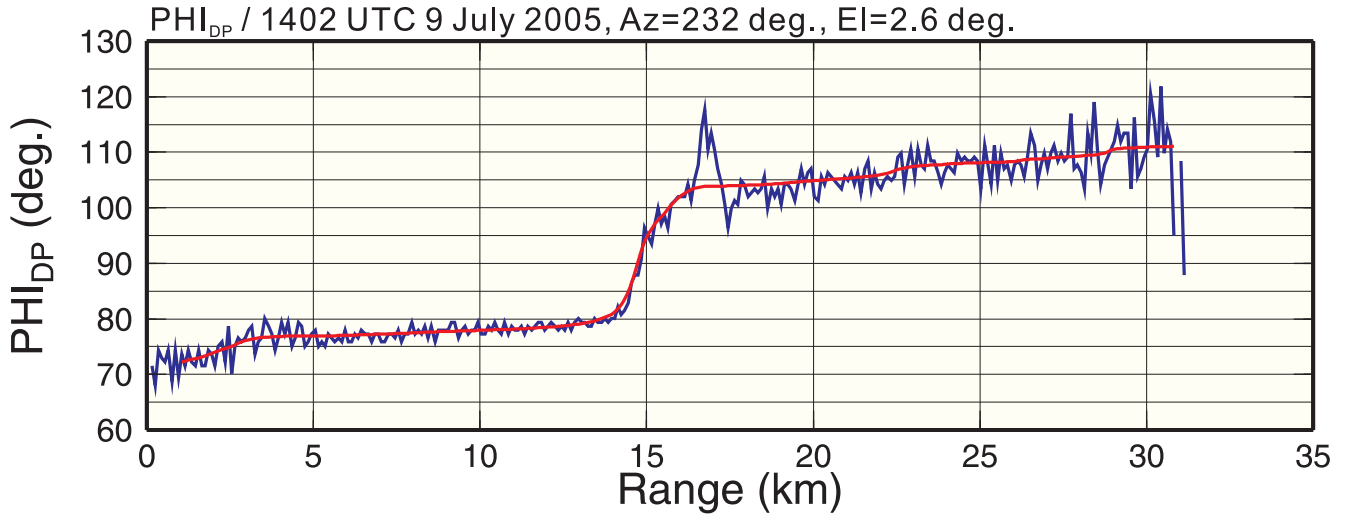


Fig. 2 The range profiles of the differential phase. Blue profile is observed by NIED's X-band dual-polarimetric radar at Ebina, Japan, at 1402 UTC 9 July 2005. The range gate width of this radar is 100 m. Red profile is analyzed from the observed data by this method ( $C_{lpf} = 1 \times 10^{11}$ ).

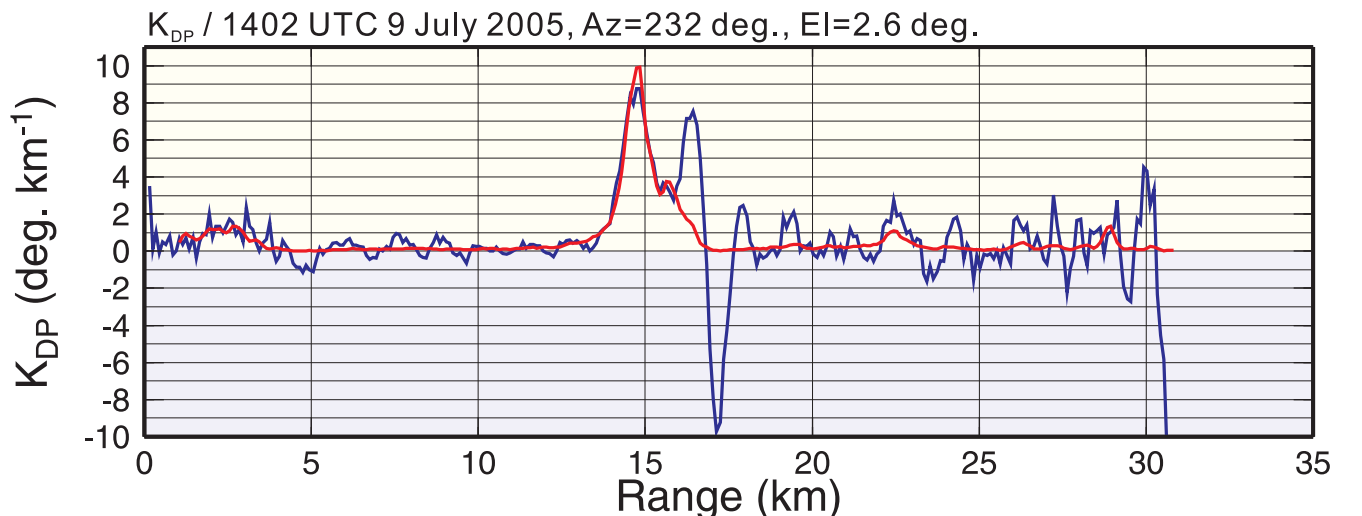


Fig. 3 The range profiles of the specific differential phase calculated from the observed differential phase shown in Fig. 2. Blue profile is estimated by the local linear regression with the regression width of 1km. Red profile is analyzed by this method ( $C_{lpf} = 1 \times 10^{11}$ ).

The dependency of the  $C_{lpf}$  is summarized in Fig. 4.

### 3. Case study

This method is applied to the NIED's X-band radar data observed at 0500 UTC 10 May 2012. Figure 5 shows the PPI images observed by the radar. At this time, narrow and high ( $\geq 50$  dBZ) reflectivity area located 20 km – 40 km northeast

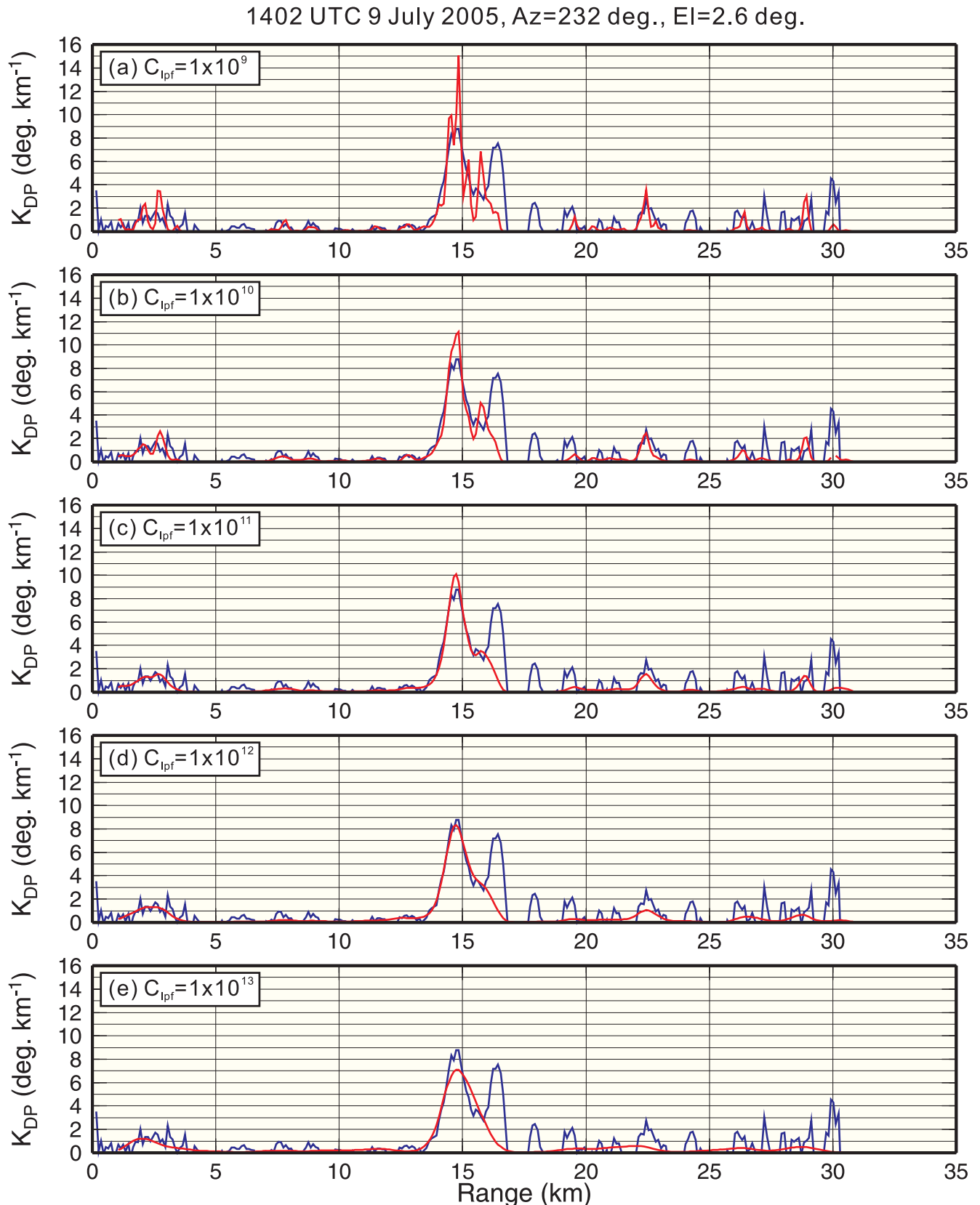


Fig. 4 Dependency of the  $C_{lpf}$  to the low pass filter in this method. The details of this figure is the same as Fig. 3. a)  $C_{lpf} = 1 \times 10^9$ , b)  $C_{lpf} = 1 \times 10^{10}$ , c)  $C_{lpf} = 1 \times 10^{11}$ , d)  $C_{lpf} = 1 \times 10^{12}$ , and e)  $C_{lpf} = 1 \times 10^{13}$ .

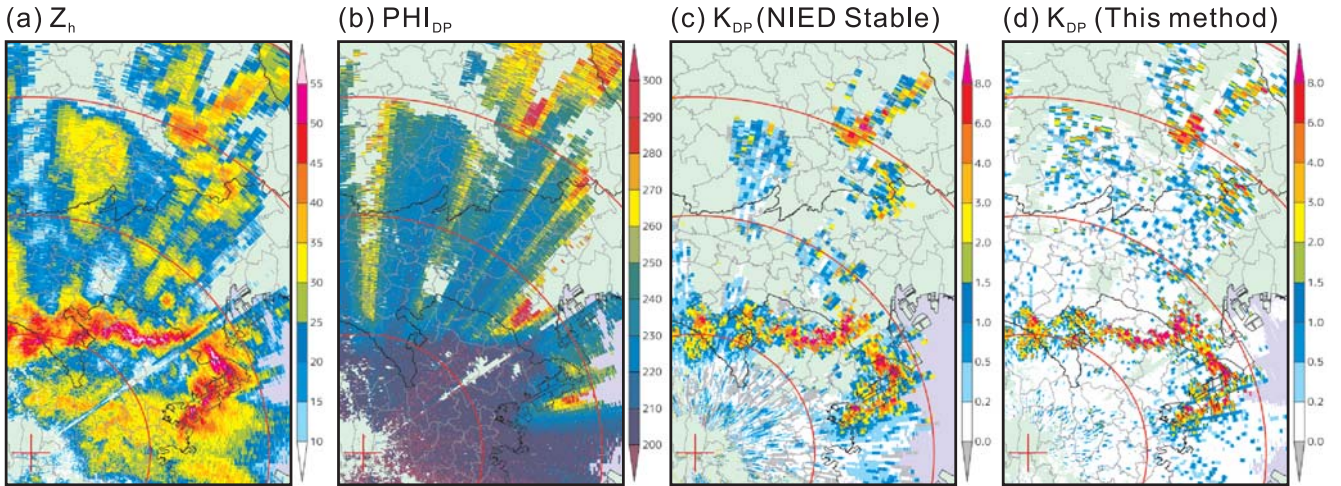


Fig. 5 PPI images of NIED's X-band polarimetric radar at Ebina city at 0500 UTC 10 May 2012. The elevation angle is  $1.2^\circ$ . Range circles are drawn at 20 km intervals from the radar. a) Observed reflectivity (no attenuation correction), b) Observed differential phase, c) Specific differential phase estimated by classic method (NIED stable algorithm: the iterative filter and local linear regression; the data which S/N ratio less than 10 dB are not used.), and d) Specific differential phase estimated by this method ( $C_{lpf} = 5 \times 10^{10}$ ).

from the radar (Fig. 5a). Figures 5c and d show the calculated  $K_{DP}$  from the  $\Phi_{DP}$  shown in Fig. 5b by the classic (NIED stable version: the iterative filter and the local linear regression) and this algorithms, respectively. Comparing this method with the classic one, the  $K_{DP}$  feature calculated by this method is narrower than that by classic method, and the high  $K_{DP}$  area ( $\geq 1.0^\circ \text{ km}^{-1}$ ) shown in Fig. 5d well corresponds to the area where the reflectivity is larger than 45 dBZ.

#### 4. Conclusions

The new method to estimate the non-negative  $K_{DP}$  for the pure rainfall was proposed. This method made the monotone increasing profile of  $\Phi_{DP}$  fitted to the observed  $\Phi_{DP}$ . The monotone increasing assumption mitigated the  $K_{DP}$  fluctuation in weak rainfall area. Furthermore the fake  $K_{DP}$  by the backscatter differential phase  $\delta$  was also suppressed, because the severe backscatter occurred locally while the fitting was done in all range. However we should take account of the backscatter differential phase in this method, in case the considerable backscatter exists in wide area. In this manner, (10) and (11) are modified as,

$$\psi_i = \Psi_i - \delta_i - \Phi_{\text{near}}, \quad (24)$$

$$\psi'_i = \Phi_{\text{far}} - \Psi_i + \delta_i. \quad (25)$$

The backscatter differential phase may be parameterized by the attenuation-corrected  $Z_{DR}$ .

By the classical  $K_{DP}$  estimation, it is difficult to perform QPE from  $K_{DP}$  for weak rainfall, because the  $K_{DP}$  fluctuation is not negligible in the weak rainfall area. So the Z-R relationship is used there. The stable and non-negative  $K_{DP}$  enables the QPE without the Z-R relationship for the weak rainfall.

#### References

- Hubbert, J. and V. N. Bringi, 1995: An interactive filtering technique for the analysis of copolar differential phase and dual-frequency radar measurements. *J. Atmos. Oceanic Technol.*, **12**, 643–648.
- Maesaka, T., M. Maki, K. Iwanami, S. Tsuchiya, K. Kieda and A. Hoshi, 2011: Operational rainfall estimation by X-band MP radar network in MLIT, Japan, *Proc. of 35th Conf. on Radar Meteorology*, Pittsburgh, 142.  
[http://ams.confex.com/ams/35Radar/webprogram/Manuscript/Paper191685/35RADAR\\_Maesaka.pdf](http://ams.confex.com/ams/35Radar/webprogram/Manuscript/Paper191685/35RADAR_Maesaka.pdf)
- Otto, T. and H. W. J. Russchenberg, 2011: Estimation of specific differential phase and differential backscatter phase from polarimetric weather radar measurements of rain, *IEEE Geosci. Remote Sens. Let.*, **8**, 988–992.
- Scarchilli, G., E. Gorgucci, V. Chandrasekar and T. A. Seliga, 1993: Rainfall estimation using polarimetric techniques at C-band frequencies. *J. Appl. Meteor.*, **32**, 1150–1160.
- Wang, Y., and V. Chandrasekar, 2009: Algorithm for estimation of the specific differential phase, *J. Atmos. Oceanic Technol.*, **26**, 2565–2578.